

uc3m | Universidad **Carlos III** de Madrid

Master Degree in Physics of Complex Systems  
2023-2024

*Master Thesis*

# “Coevolution of Synchronization and Cooperation on Spatio-Temporal Networks”

---

Michele Lambresa

Supervisor: Alberto Antonioni

Co-supervisor: Luca Dall’Asta

Madrid, 15/06/2024



Politecnico  
di Torino



Université  
Paris Cité



UNIVERSITÉ FRANCO ITALIO  
ITALIENNE UNIVERSITÀ FRANCESE



## **ABSTRACT**

The spontaneous emergence of synchronization across various natural systems witnesses its importance in executing complex collective tasks within a population. Similarly, cooperation is a crucial behavioral mechanism for ensuring the survival of a community in numerous physical, biological, and social scenarios. Despite the evident interplay between synchronization and cooperation in many real-world systems, a rigorous investigation of their relationship has seldom been conducted. The Evolutionary Kuramoto Dilemma offers a quantitative approach to study the coevolution of cooperation and synchronization within the framework of networked interactions among populations of coupled oscillators/agents. Each individual may decide whether or not to cooperate and interact with the rest of the population in order to get synchronized. The decision is based on the benefit-to-cost ratio they accrued in the past: cooperating means contributing to the collective benefit of synchronization but also incurring the individual cost of interactions. We investigate the onset of synchronization and cooperation within this framework, emphasizing how different interaction topologies significantly influence the emerging phenomena. Following an initial investigation on static networks, our analysis shifts to spatio-temporal networks, aiming to identify the conditions under which mobile individuals and dynamical interactions promote synchronization and cooperation.

# CONTENTS

1. INTRODUCTION . . . . .	1
2. METHODS . . . . .	3
2.1. Kuramoto Model . . . . .	3
2.2. Evolutionary Games . . . . .	6
2.3. Evolutionary Kuramoto Dilemma . . . . .	7
2.4. Complex Networks. . . . .	9
2.4.1. Erdős-Rényi Graph (ER) . . . . .	9
2.4.2. Random Geometric Graph (RGG) . . . . .	9
2.4.3. Temporal Proximity Graph (TPG) . . . . .	10
2.5. Simulation setup . . . . .	11
3. RESULTS . . . . .	12
3.1. Analytical conditions . . . . .	12
3.2. Static networks . . . . .	14
3.3. Temporal proximity graphs . . . . .	17
4. CONCLUSION . . . . .	21
BIBLIOGRAPHY. . . . .	22

# 1. INTRODUCTION

The second law of thermodynamics tells us that everything in the universe tends towards disorder. If we consider complex systems—the closest representation of real-world systems—, we expect this principle to be even more evident. Conversely, we continually experience occasions of spontaneous order even in everyday life: the regular beating of our heart, the repeated contraction of the diaphragm, the simultaneous firing of brain neurons, the perfectly timed orbits of moons, the concurrent flashing of fireflies, the hypnotic murmuration of starlings, or even the coordinated actions of groups of individuals [1]. Natural systems tend to work in rhythm, suggesting that a coherent collective behavior enforces their robustness, strengthening the bonds among individuals and facilitating the achievement of much more complicated tasks. This fascinating self-organization is commonly known as *synchronization*.

The most appealing aspect of this phenomenon is how universal it is, occurring at every scale of nature and exploiting mechanical, chemical, electrical, gravitational and many other communication channels to emerge. In this perspective, scientists have been investigating synchronization phenomena for a long time, aiming to provide a unified quantitative description of the mechanisms governing this behaviors.

A standard approach to tackle this problem is to describe the physical, technological, biological, or social system under consideration as a population of coupled *phase oscillators*. Each oscillator swings with a specific frequency and modifies its rhythm depending on the interactions with the rest of the population. The nature and the structure of the communication within the population depends on the context under investigation, resulting in a rich spectrum of diverse dynamics. If the interaction are sufficiently suitable, the oscillators manage to converge their oscillations towards a common frequency. As a result, the whole population synchronizes.[2]

In physics, interacting systems are usually described by considering each component of the population as a passive dynamical unit bound to obey the governing laws of its evolution. However, it is evident that many real-world situations do not match such a description. In biological, economical, social contexts, populations are rather composed by *active agents*, capable of making rational decisions and adopting different strategies, attempting to meet their personal needs. Individuals may be in conflict, pursuing the same or a different objective; they may have different opinions, persuade the partners to adopt their strategies or even behave irrationally.

Among the behavioral mechanisms emerging in systems of active agents, one of the most interesting is certainly *cooperation*. The altruistic act of helping each other is counterintuitive, especially when agents seek to achieve their own personal success. Yet, many biological and social populations decide to cooperate even in selfish scenarios, where cooperating is costly but provides a greater collective benefit. This highlights cooperation as a crucial behavior to ensure the community's survival.

The powerful tool addressing this phenomenon is known as *evolutionary game theory* [3]. Game theory is the unifying paradigm that provides a rigorous methodology to describe decision-making processes. In this framework, the interacting units are considered to be rational "players" facing a *dilemma*, i.e. a strategic decision. The agent's choice eventually leads to a personal loss or gain

depending on its effectiveness. The dilemma is commonly figured out by a game each agent plays against another member of the population, where its eventual gain, or victory, implies a loss, or defeat, for the opponent. Individuals play several rounds against various opponents and each of them eventually ends up with a net gain or loss depending on the adopted strategy.

Unlike its classical counterpart, evolutionary game theory allows agents to change their strategy over time. Individuals can learn from other agents and imitate those adopting more successful strategies. As a result, during the dynamics, convenient strategies survive while inefficient strategies die out. The resulting selection mechanism becomes particularly interesting when the strategies to be adopted are cooperation and defection. In this perspective, evolutionary games are exploited to investigate the onset of this collective behavior [4].

Real-world systems exhibit extremely complex patterns of interaction. In recent years, the exploration of complex systems has propelled significant advancements in the investigation of topologies where individual units interact solely with a subset of the entire population. Among these advancements, *network science* stands out as one of the most relevant. In this perspective, a population is visualized as a large interconnected network, where each unit is represented by a node and interacts with the connected neighbors. The way the network is constructed depends on the context under examination, indicating a wide range of different structures [5]. In social sciences and biology, as well as in physics and engineering, the communication usually relies on the physical proximity among the individuals: the closer two individuals are in space, the stronger will be their interaction. On the other hand, in real contexts, individuals typically are not static entities, but rather dynamical units that modify their interactions over time. Each unit dynamically changes its partners and adapts its communication accordingly. To describe such a scenario, the paradigmatic framework employs *spatio-temporal networks*.

The attempt of merging together synchronization phenomena, evolutionary game theory and complex networks appears noteworthy. From the above overview, synchronization and cooperation result both in pivotal mechanisms in nature, often emerging as counterparts to each other. Investigating their interplay within complex networks is essential to accurately replicate real-world contexts.

In the present study, we investigate the coevolution of synchronization and cooperation when the oscillators are active agents that can decide whether or not to interact, i.e. cooperate, with the rest of the population. The interactions are costly, but provide the collective benefit of mutual synchronization. To address this scenario, we employ the model introduced by Antonioni *et al.*, called *Evolutionary Kuramoto Dilemma* [6]. After a preliminary part devoted to reproducing the results already introduced in [6] for static networks, the novel analysis will be focused on the behavior of the model on spatio-temporal networks.

This report is organized in three main parts. Chap. 2 is devoted to the rigorous introduction of the model and the employed methods. In chap. 3 we present the final outcomes of our analysis. Finally, chap. 4, provides a brief summary of the work and proposes potential future advancements.

## 2. METHODS

Integrating decision-making processes into the dynamics of networked-interacting oscillators naturally merges synchronization with evolutionary game theory. The model studied in this work, called Evolutionary Kuramoto Dilemma, embodies this coevolutionary approach. To understand how synchronization phenomena and evolutionary dynamics can be combined, it is essential to first present each subject separately: this is the aim of sec. 2.1 and 2.2., while sec. 2.3 introduces the principal model. Sec. 2.4 describes the employed topologies. Finally, sec. 2.5 briefly outlines the simulation setup.

### 2.1. Kuramoto Model

Due to its broad phenomenology in several different contexts, collective synchronization has been explored through numerous approaches. Among all, the model proposed by Kuramoto (1975) stands out as the most successful attempt to provide a general description of the phenomenon, owing to its mathematical tractability while retaining a nontrivial complexity.

In this framework, synchronization is addressed as the ability of a population of weakly-coupled, nearly identical, interacting phase oscillators to adjust their rhythms based on the interaction with each other, eventually leading them to share a common frequency (*phase-locking*). The emergence of a fully synchronized state occurs only if the strength of the coupling is sufficient to overcome the diversity in the oscillators' natural frequencies; otherwise the system falls into a completely incoherent regime. As a matter of fact, the phenomenology is analogous to an equilibrium phase transition: the system alters its collective behaviour beyond a critical threshold of the coupling strength.

Over the past forty-five years, the Kuramoto model has been subject to intensive study, resulting in the proposal of several variations [2]. In the following paragraphs, the focus will be on presenting the aspects that are most relevant to the current work.

#### Mean-Field case

The original model worked out by Kuramoto employs a mean-field approach. It consists of a population of  $N$  phase oscillators  $\theta_i(t)$  which are coupled by an all-to-all sinusoidal term. Each oscillator tries to run by its natural frequency while the coupling tends to synchronize it to all the others. Thus the dynamics is governed by the following nonlinear ODEs' system:

$$\dot{\theta}_i = \omega_i + \frac{\lambda}{N} \sum_{j=1}^N \sin(\theta_j - \theta_i), \quad i = 1, \dots, N \quad (2.1)$$

where the factor  $1/N$  ensures a good behaviour in the thermodynamic limit  $N \rightarrow \infty$ ,  $\lambda$  is the coupling strength, and  $\omega_i$  denotes the natural frequency of oscillator  $i$ . The frequencies  $\omega_i$  are i.i.d. random variables following the probability density  $g(\omega)$ , assumed to be unimodal and symmetric with respect to its mean frequency  $\Omega$ . One can set  $\Omega=0$  without loss of generality, since a suitable choice of the

rotating frame  $\omega_i \rightarrow \omega_i + \Omega$  for all  $i$  is always possible.

The collective behaviour of the whole population is measured by the *macroscopic* complex order parameter:

$$r_G(t)e^{i\psi(t)} = \frac{1}{N} \sum_{j=1}^N e^{i\theta_j(t)} \quad (2.2)$$

where  $\psi(t)$  is the average phase and the modulus  $r_G(t)$  measures the coherence of the global state:  $r_G \simeq 1$  indicates a fully synchronized state whereas  $r_G \simeq 0$  describes a totally incoherent motion of the oscillators. Intermediate values of  $r_G$  suggest a partially coherent global state, where a group of oscillators is phase-locked, while the rest of the population remains incoherent.

By this definition, employing the Euler's identity, Eqs. 2.1 can be decoupled and rewritten as:

$$\dot{\theta}_i = \omega_i + \lambda r_G \sin(\psi - \theta_i), \quad i = 1, \dots, N \quad (2.3)$$

Eq. 2.3 clarifies the significance of the order parameter, indicating that each oscillator is coupled to the average phase  $\psi(t)$  through a coupling strength  $\lambda r_G$ .

To infer the value of the critical coupling, a self-consistent equation for  $r_G$  can be derived starting from Eq. 2.3, admitting a nontrivial solution  $r_G > 0$  when the coupling strength exceeds a certain threshold [7]. The resulting bifurcation point occurs at:

$$\lambda_c^{MF} = \frac{2}{\pi g(0)} \quad (2.4)$$

This value represents the mean-field critical coupling and we have verified it by the numerical simulation shown in figure 2.1. This last result is the starting point to infer the critical coupling on complex networks

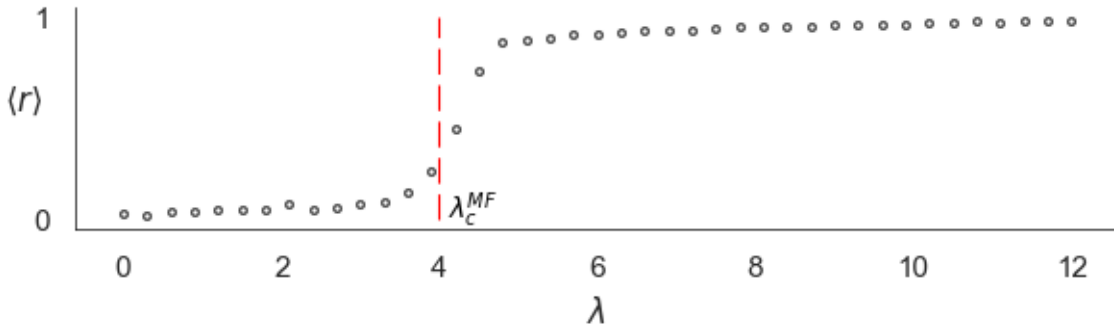


Fig. 2.1. Numerical realization of the bifurcation diagram for a population of 1000 oscillators whose natural frequencies are uniformly distributed in  $[-\pi, \pi]$ . The red dashed line represents the corresponding critical coupling  $\lambda_c^{MF} = 4$ . The results are averaged over 10 realizations.

## Kuramoto Model on complex networks

Despite the mean-field Kuramoto Model offers an initial framework for understanding the onset of synchronization, its major drawback lies in the assumption that each oscillator communicates with every other unit in the population. This assumption is difficult to conceive in real-world systems.

In a more realistic framework, the pattern of interactions governing the dynamics is described by a

complex network, where each oscillator interacts exclusively with its connected neighbors. For the sake of clarity, the number of neighbors is commonly referred to as the *degree* of the node.

There are countless ways to construct such a network, but we will delve into these techniques in the later sections. For now, it is sufficient to understand that networks can be mathematically described as graphs, whose connectivity is represented by the so-called *adjacency matrix*. The element  $a_{ij}$  of the matrix is equal to 1 if node  $i$  is connected to node  $j$ , otherwise it is equal to 0.

Variations in the topology dramatically affects the phenomenology of the Kuramoto Model (KM), leading to different types of phase transitions, altering the critical coupling values, or even precluding the possibility of a synchronized state. The first challenge in designing KM on complex networks is how to define the coupling term. Unlike the mean-field case, there are several possible choices. Following [8], the selected prescription consists in the following definition:

$$\dot{\theta}_i = \omega_i + \lambda \sum_{j=1}^N a_{ij} \sin(\theta_j - \theta_i), \quad i = 1, \dots, N \quad (2.5)$$

where  $a_{ij}$  is the element of the graph's adjacency matrix, while  $\lambda$  is implicitly rescaled by the maximum degree  $k$  of the network, i.e.  $\lambda = \lambda_A/k_A = \lambda_B/k_B$  for two different topologies A and B. This rescaling allows for comparison between different networks, as it projects their dynamics onto the same timescale. It also guarantees good behavior in the thermodynamic limit and it preserves the topological heterogeneity, unlike other prescriptions [8].

Complex networks also require more attention when measuring the collective behavior of the system. In addition to the macroscopic order parameter introduced in Equation 2.2, a microscopic version can be defined to assess the level of local synchronization of each node with its neighbors. In the same spirit as Equation 2.2, considering two linked nodes  $l$  and  $m$ , we define a pairwise measure:

$$r_{lm} e^{i(\theta_l + \theta_m)/2} = \frac{e^{i\theta_l} + e^{i\theta_m}}{2} \quad (2.6)$$

Hence, for a node  $l$ , the *local* order parameter  $r_l$  is defined as:

$$r_l = \frac{\sum_{m=1}^N a_{lm} r_{lm}}{k_l} \quad (2.7)$$

where  $k_l = \sum_m a_{lm}$  is the degree of node  $l$ . By its definition,  $r_l \simeq 1$  when the phase  $\theta_l$  is concurrently close to the phases of its neighbors; in the opposite case it approaches 0.

Lastly, the *microscopic* order parameter for the whole population can be written as the average of the local parameters over all nodes:

$$r_L = \frac{1}{N} \sum_{l=1}^N r_l \quad (2.8)$$

The meaning of  $r_L$  is substantially different from the macroscopic one, as it provides insight into the synchronization level of each cluster of neighboring nodes in the network. This measure can approach 1 even if a global coherent state is not reached, indicating the formation of several groups of phase-locked oscillators, i.e. when the so-called *chimera state* emerges [9].

The last noteworthy finding presented in this section concerns the variation of the critical coupling value when dealing with complex networks. By employing a mean-field approximation, the critical coupling can be derived analytically even when the topology is different from a complete graph [10].

The surprising finding reveals that the critical mean-field value is simply rescaled by the ratio of the first two moments of the graph's degree distribution, regardless of the many other differences among the topologies:

$$\lambda_c^{th} = \lambda_c^{MF} \frac{\langle k \rangle}{\langle k^2 \rangle} \quad (2.9)$$

where  $\langle k \rangle$  is the average number of neighbors and  $\langle k^2 \rangle$  is the second moment of the degree distribution. This theoretical value will be used for subsequent comparisons with the results presented in chap. 3.

## 2.2. Evolutionary Games

As previously mentioned, decision-making processes are commonly investigated through evolutionary game theory, where individuals are active agents that can adopt different strategies based on their purpose. Since we want to characterize cooperation phenomena, let us assume two possible strategies: cooperation and defection. Cooperation means that the agent accepts to interact with the rest of the population, while defectors refuse to communicate.

The effectiveness of each strategy is evaluated by the net gain or loss the agent accumulates during time, referred to as its *payoff* [4]. The higher the payoff, the more successful the agent's strategy. For cooperation phenomena, the standard way payoffs are measured is in terms of costs and benefits. A cooperator pays a cost  $c$  to perform the altruistic act but provides a collective benefit  $b$  to all the community it interacts with. Conversely, a defector does not incur any cost, rejecting to contribute to the collective welfare ( $c = 0$ ). Hence the payoff  $\Pi$  of each agent can be written as:

$$\Pi = b - c \quad (2.10)$$

It is intuitive that a defector is intrinsically advantaged compared to a cooperator, as it receives the benefit provided by the cooperators without paying any cost, thus accumulating a higher payoff. This scenario is referred to as an *evolutionary noncooperative game*.

As introduced in Chap. 1, the dynamics of evolutionary games is characterized by agents' capability to change their strategy over time. The time evolution of the system yields to the emergence of the successful strategies, implying that ineffective ones disappear. In this perspective, agents are able to imitate the strategy of successful individuals, aspiring to achieve a higher payoff. The latter evolutionary dynamics is called *replicator dynamics* [3].

The selection rule by which a player changes its strategy can be designed in many different ways. The simplest one relies on the mere difference between the payoffs of the player and the opponent: 'if the opponent's payoff is higher than mine, then I will imitate its strategy'. This corresponds to the deterministic case of agents' full rationality. However, it seems more realistic to include "noisy effects" in agents' decision-making process, as they are not always sure to make the right choice. To take into account this aspect, the so-called *Fermi rule* is much more appropriate. According to the rule, the probability that player  $A$ , with payoff  $\Pi_A$  and strategy  $s_A$ , imitates the strategy of player  $B$ , with payoff  $\Pi_B$  and strategy  $s_B$ , is distributed according the logistic function:

$$P(s_A \leftarrow s_B) = \frac{1}{1 + e^{-\beta(\Pi_B - \Pi_A)}} \quad (2.11)$$

where  $\beta$  stands for the "irrationality" of the players. Evidently, the more the payoff of B exceeds that of A, the more probable A will imitate B. The role of  $\beta$  in Eq. 2.11, is that of tuning the randomness

of the selection rule. For high values of  $\beta$ , the Fermi rule tends to the full rationality case. While for low values of  $\beta$ , the decision approaches a random choice.

### 2.3. Evolutionary Kuramoto Dilemma

Here we ultimately present the model investigated in our work. The Evolutionary Kuramoto Dilemma (EKD), first proposed by Antonioni and Cardillo in 2017 [6], is the pioneering work that studies the emergence of synchronization by associating a cost to the networked interactions within a population of oscillators.

In this framework, each oscillator acts as an agent that can choose between two strategies:

- *Cooperation*: the oscillator accepts to interact with its neighbors in a Kuramoto-like manner, trying to reach mutual synchronization.
- *Defection*: the oscillator refuses to interact, free-riding at its natural frequency regardless of the rest of the population.

The model aims to investigate how cooperation and synchronization *coevolve*, meaning that the two aspects mutually influence each other.

Formally, let us consider a graph  $G$  of  $N$  nodes, where each node  $l$  is a dynamical unit defined by its phase  $\theta_l$  and strategy  $s_l \in \{0, 1\}$ . The strategy is set to  $s_l = 1$  if the agent is a cooperater,  $s_l = 0$  if it is a defector. The discrete dynamics of the system is designed so that, at each instant of time, the two variables  $\theta_l$  and  $s_l$  are updated through two distinct but communicating processes: the *synchronization step* and the *game step*. These processes are described separately in the following two paragraphs. In the third paragraph the whole dynamics is presented, focusing on how the stationary state is investigated.

#### Synchronization step

The phase update is performed within this step. In the spirit of the Kuramoto model, the phase dynamics of each oscillator is described by the following differential equation:

$$\dot{\theta}_l = \omega_l + s_l \lambda \sum_{j=1}^N a_{lj} \sin(\theta_j - \theta_l) \quad (2.12)$$

where  $\omega_l$  is the natural frequency,  $s_l$  the strategy of the node  $l$ ,  $a_{lj}$  the element of the adjacency matrix of  $G$  and  $\lambda$  the coupling strength. From Eq. 2.12, it is evident that the nonlinear coupling term is included only in the dynamics of cooperaters, enabling them to adjust their own rhythm and synchronize with their neighbors. Conversely, if the node is a defector, it oscillates undisturbed at its natural frequency.

The evolution of the phase trajectory is numerically computed with the Runge-Kutta 4th-Order method.

## Game step

The strategy update is performed within this step. In the framework of sec. 2.2, each oscillator  $l$  is assigned a payoff  $\Pi_l$  that quantifies the balance between the cost  $c_l$  and the benefit  $b_l$ .

The definition of cost and benefit is closely tied to the previously described synchronization dynamics. The collective benefit that each agent gains is simply the level of synchronization between the node and its neighbors, represented by the local order parameter defined in Equation 2.7:

$$b_l(t) \equiv r_l(t) \quad (2.13)$$

The individual cost a cooperator has to pay is defined by how much the oscillator has modified its frequency to converge towards local synchronization within a time step  $\epsilon$ . Hence, it is given by the absolute value of the angular acceleration:

$$c_l(t) = \Delta\dot{\theta}_l \equiv |\dot{\theta}_l(t) - \dot{\theta}_l(t - \epsilon)| \quad (2.14)$$

Let us emphasize that while the benefit is earned by all oscillators, irrespective of the employed strategy, the cost is incurred only by cooperators, since defectors do not alter their natural frequency over time. Therefore the system is placed within the framework of an evolutionary noncooperative game (sec. 2.2).

As a result, the payoff attained by the agent  $l$  is naturally evaluated as the difference between these two quantities:

$$\Pi_l(t) = b_l(t) - \alpha \frac{c_l(t)}{2\pi} \quad (2.15)$$

where  $\alpha$  is the *relative cost* and  $2\pi$  is a scaling factor. The independent variable  $\alpha$  acts as a control parameter, tuning the system from a regime of cheap interactions to one of expensive interactions. The criterion by which each agent selects its strategy over time is governed by the replicator dynamics introduced in section 2.2. During the game step, each agent  $l$  randomly selects one of its neighbors,  $m$ , and replicates its strategy with a certain probability, according to the previously-mentioned Fermi rule:

$$P(s_l \leftarrow s_m) = \frac{1}{1 + e^{-\beta(\Pi_m - \Pi_l)}} \quad (2.16)$$

where  $\beta$  is the "irrationality" of the agents. The strategy update occurs in a *synchronous* manner, i.e. all agents play the game with their current strategy  $s_l(t)$ , even though they have already decided which strategy to adopt in the next time step  $s_l(t + \epsilon)$  by a previous match.

## Global dynamics

The temporal evolution of the entire system is thus determined by the iteration of the two processes over time: at each time step, a synchronization step updates the phases of the oscillators, and subsequently, after the agents have accumulated their payoffs, a game step updates their strategy. This protocol continues until the system reaches the stationary state.

To assess the emergent collective behaviour of the population, three order parameters are employed: the canonical macroscopic and microscopic level of synchronization,  $r_G$  and  $r_L$ , respectively defined by Eqs. 2.2 and 2.8, and the average number of cooperators  $C = \frac{1}{N} \sum_l s_l$ .

## 2.4. Complex Networks

To achieve a closer representation of real-world systems, it is fundamentally important to study the dynamics of interacting populations models on complex networks, examining how the pattern of interactions affects their collective behavior.

In the present study, a complex network is mathematically referred to as a graph  $G(N, \langle k \rangle)$ , where  $N$  represents the number of nodes and  $\langle k \rangle$  denotes the average number of neighbors, i.e. the average degree. The nodes are connected by edges that shape the interactions within the population. The edges are *undirected* and *unweighted*, i.e. they do not have a specified directionality and they all possess equal significance. Additionally, the graphs are *homogeneous*, meaning that the tail of the degree distribution  $P(k)$  decays exponentially fast. This implies that the degree of each node fluctuates around the mean value  $\langle k \rangle$ , avoiding large deviations [5].

This section outlines the networks considered in this work, particularly focusing on the derivation of  $\langle k \rangle$ , a fundamental parameter for the further analysis. The three chosen topologies are profoundly different in nature, leading to substantial differences in the population's evolution.

### 2.4.1. Erdős-Rényi Graph (ER)

The Erdős-Rényi graph (ER), also known as *random graph*, was first introduced by the Hungarian mathematicians Paul Erdős and Alfréd Rényi in 1959 [11]. The graph represents the first attempt to describe a complex network with connectivity generated by a random process.

In our work, a ER graph with  $N$  nodes is constructed by including each edge in the graph with a fixed probability  $p$ , independently of the other edges. From a probabilistic perspective, each edge is a Bernoulli random variable. Consequently, the probability that the node  $l$  has  $k$  edges (neighbors) follows a Binomial distribution:

$$P(k_l = k) = \binom{N-1}{k} p^k (1-p)^{N-1-k} \quad (2.17)$$

where  $(N-1)$  is the maximum number of edges a node can possess. As a result, the average degree is given by:

$$\langle k \rangle = p(N-1) \quad (2.18)$$

### 2.4.2. Random Geometric Graph (RGG)

Random graphs, like other classes of networks, can be considered *relational networks*, where the concept of physical distance is not relevant. These topologies are particularly useful to describe many real-world systems where interacting units communicate equally, regardless of whether they are close or distant nodes. This is especially true in the age of the Internet and the World Wide Web.

On the contrary, many systems base their pattern of interactions precisely on spatial constraints. Consider, for example, neuronal networks, electric power grids, transportation systems or human societies. To describe such systems, a particular class of graphs is used, where nodes are embedded in physical space, and edges depend on the spatial distance between them. These networks are called *spatial networks* [12].

The random geometric graph (RGG) is the standard model for spatial networks, serving a similar role as the ER random graph for relational networks. In this study, the structure of a RGG with  $N$  nodes and *interaction radius*  $R$  is governed by the two following rules [13]:

- (1) The  $N$  nodes are uniformly distributed in the unitary square  $[0, 1]^2 \in \mathbb{R}^2$ .
- (2) An edge is created for every pair of nodes  $(i, j)$  within the Euclidean distance  $d_{ij} < R$ . The periodic boundary conditions are assumed, meaning the unitary space is boundless (*torus*).

By this prescription, a RGG can be visualized as a square filled with small circles of radius  $R$  and area  $V = \pi R^2$ : the edges are established only between the circles that overlap. Accordingly, the average degree can be estimated by the formula  $\langle k \rangle = \rho V$ , where  $\rho$  is the number of nodes per unit space [14]. In our case,  $\rho = N$  since the unitary square is considered. Hence, in order to construct a RGG with average degree  $\langle k \rangle$ , it is sufficient to set the radius  $R$  properly:

$$R = \sqrt{\frac{\langle k \rangle}{\pi N}} \quad (2.19)$$

Let us emphasize the effect of spatial correlations in RGG networks. The constraint that nodes can only interact within a radius  $R$  causes nodes to organize into clusters of interactions. Specifically, if node  $i$  is connected to nodes  $j$  and  $k$ , it is very likely that nodes  $j$  and  $k$  are also connected. This feature makes RGGs and ERs fundamentally different. Fig. 2.2 provides a visual comparison of the two structures.

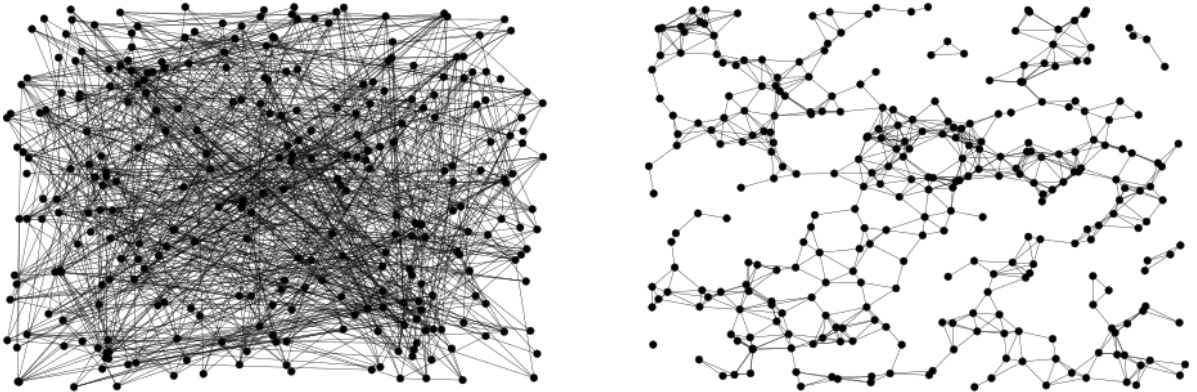


Fig. 2.2. ER (left panel) and RGG (right panel) topologies for  $N = 300$  nodes and average degree  $\langle k \rangle = 6$ .

### 2.4.3. Temporal Proximity Graph (TPG)

A notable characteristic of many biological, engineering, economic, and social systems is that the interactions between their components are not static but exhibit explicit temporal dynamics. To represent these evolving interactions, it is customary to use specialized graphs whose topological properties change over time. These graphs are typically referred to as *temporal networks* [15].

In the context of spatial graphs, temporal networks allow component units to move within the physical space they inhabit, according to a specific motion law. Their movement alters the pattern of interactions based on the partners they encounter along the way. These graphs are commonly called *spatio-temporal networks*.

Among such mobile networks, the paradigmatic model we focus on is the temporal proximity graph (TPG) [16]. In the present work, TPGs are the time-varying counterpart of RGGs, as their edge generation rule are identical: at each instant of time, nodes within a certain distance threshold  $R$  are connected. The substantial distinction between the two models is that, unlike RGG, TPG nodes are 2D random walkers moving freely throughout the boundless unitary space [17].

Formally, each node  $l$ , spatially described by its position  $\mathbf{x}_l(t)$ , moves at time  $t$  with a velocity  $\mathbf{v}_l(t)$ . The nodes can only change their direction of motion  $\varphi_l(t)$ , while their speed  $v$  remains constant in time. Hence the velocity can be written as  $\mathbf{v}_l(t) = [v \cos(\varphi_l(t)), v \sin(\varphi_l(t))]$ . As random walkers, the directions of motion are randomly sampled at each time step. Initially, the positions  $\mathbf{x}_l(0)$  are uniformly distributed in the unitary square  $[0, 1]^2$ . The discrete temporal evolution of the system thus is governed by the following motion laws:

$$\mathbf{x}_l(t + \epsilon) = \mathbf{x}_l(t) + \mathbf{v}_l(t) \quad (2.20)$$

$$\varphi_l(t + \epsilon) = \eta_l \quad (2.21)$$

where  $l = 1, \dots, N$ ,  $\epsilon$  is the time step size and  $\eta_l$  are  $N$ -independent random variables with uniform distribution in the interval  $[0, 2\pi]$ .

The choice of the speed  $v$  profoundly affects how node connectivity changes over time. Values of  $v \ll R$  mean that nodes fluctuate around their initial positions, maintaining more or less the same edges throughout the evolution. Conversely,  $v \gg R$  indicates that the neighborhoods are continuously reset. Hence it is reasonable to highlight how the value of the speed compares to the interaction radius  $R$ . In light of this, we define the *relative mobility*  $\mu$  so that:

$$v = \mu R \quad (2.22)$$

where  $R$  is defined by Eq. 2.19. The relative mobility  $\mu$  is an independent variable and will play the role of a control parameter in the further analysis.

## 2.5. Simulation setup

We schematically outline the settings of the employed free parameters in the numerical implementation of the EKD model. The simulations are performed on a population of  $N = 1000$  oscillators/agents. For each dynamical unit  $l$ , the initial phase  $\theta_l(0)$  and the natural frequency  $\omega_l$  are drawn independently from a uniform distribution in the interval  $[-\pi, \pi]$ , while the strategy  $s_l(0)$  is randomly initialized between 0 and 1. To ensure the correct functioning of the Runge-Kutta 4th-order method, the time step size is fixed at  $\epsilon = 0.01$ . Without loss of generality, the irrationality of the agents is chosen to be  $\beta = 1$ . The average degree of the various networks is commonly set to  $\langle k \rangle = 6$ .

### 3. RESULTS

This chapter is dedicated to the outline and the analysis of the results obtained by extensive numerical simulations of the EKD model. We organized the analysis in three sections. Sec. 3.1 derives some preliminary analytical results. Sec. 3.2 focuses on the study of the ER and RGG static cases. Finally sec. 3.3 investigates the EKD on TPGs.

#### 3.1. Analytical conditions

The design of the EKD model, as it integrates nonlinear ODEs, decision processes, and complex networks, makes the derivation of analytical results highly complicated. Nevertheless, we present some theoretical outcomes that are invaluable for validating and enhancing the subsequent numerical findings [18].

##### Lower bound for the microscopic order parameter

It is possible to estimate the value of the microscopic order parameter  $r_L$  (Eq. 2.8) in the scenario of total defection, where all the oscillators run incoherently. This evaluation translates in computing the average value of the pairwise measure  $r_{lm}$  defined in Eq. 2.6, as  $r_L$  implicitly consists in a refined average of this measure across the entire network.

Let us consider the phases  $\theta_l$  and  $\theta_m$  of two randomly selected oscillators  $l$  and  $m$  among the population. Rotating the reference frame by an angle  $-\theta_l$ , we perform a change of coordinates to  $\theta'_l = 0$  and  $\theta'_m = \theta_m - \theta_l = \theta$ . Hence the pairwise measure can be written as  $r_{lm} = |1 + e^{i\theta}|/2$ . Considering the limiting case of totally incoherent motion, we can assume that  $\theta$  follows a uniform distribution over  $[-\pi, \pi]$ . The average pairwise measure  $\overline{r_{lm}}$  thus is given by:

$$\begin{aligned} \overline{r_{lm}} &= \frac{1}{2\pi} \int_{-\pi}^{\pi} \frac{|1 + e^{i\theta}|}{2} d\theta = \frac{1}{2\pi} \int_{-\pi}^{\pi} \frac{|1 + \cos\theta + i\sin\theta|}{2} d\theta = \frac{1}{2\pi} \int_{-\pi}^{\pi} \frac{\sqrt{(1 + \cos\theta)^2 + \sin^2\theta}}{2} d\theta \\ &= \frac{1}{2\pi} \int_{-\pi}^{\pi} \sqrt{\frac{1 + \cos\theta}{2}} d\theta = \frac{1}{2\pi} \int_{-\pi}^{\pi} \cos(\theta/2) d\theta = \frac{4}{2\pi} = \frac{2}{\pi} \approx 0.6366 \end{aligned} \quad (3.1)$$

The last result represents a qualitative lower bound for the microscopic order parameter. We expect to encounter approximately this value whenever the system reaches a stationary state characterized by a fully incoherent behavior.

##### Prerequisites for the onset of cooperation

It is possible to estimate the limiting conditions under which cooperation can emerge. To do so, Ohtsuki *et al.* proposed a simple rule to establish the evolutionary scenarios favoring cooperation in

networked populations [19]. This rule is given by the condition:

$$\frac{b}{c} > \langle k \rangle \quad (3.1)$$

where  $\langle k \rangle$  is the average degree,  $b$  is the net benefit achieved by being a cooperator rather than a defector, and  $c$  is the cost of this altruistic act.

In our case, let us consider the extreme scenario of a network consisting of only two oscillators,  $C$  and  $D$ ,  $C$  being a cooperator and  $D$  a defector. Let  $\theta_C$ ,  $\theta_D$  and  $\omega_C$ ,  $\omega_D$  be the corresponding phases and natural frequencies. Without loss of generality, we assume  $\omega_C$  to be equal to the average frequency  $\Omega = 0$ . In addition, with the same logic as in the previous paragraph, we set  $\theta_D = 0$  by rotating the reference frame.

According to the selection rule of Eq. 2.15,  $C$  will pay a cost  $c$  to provide a collective benefit to both the oscillators. At each time step, the net benefit  $b$  that  $D$  receives from  $C$  is equal to  $b = b_C - b_D$ , representing the benefit resulting from  $C$ 's choice to cooperate ( $b_C$ ), rather than defect ( $b_D$ ). Let us calculate each quantity separately.

As in the previous paragraph, in a scenario of total defection the benefit  $b_D$  is given by:

$$b_D = r_{lm} = \frac{|1 + e^{i\theta}|}{2} = \sqrt{\frac{1 + \cos(\theta_C(t))}{2}} \quad (3.2)$$

Conversely, when one oscillator switches strategy to become a cooperator, it will modify its phase according to Eq. 2.12. At each time step, we have:

$$\theta_C(t + \epsilon) = \theta_C(t) + \epsilon\lambda \sin(-\theta_C(t)) \quad (3.3)$$

where  $\epsilon$  is the discrete time step size and  $\lambda$  the coupling strength. As a result, the benefit  $b_C$  provided to the whole system at each time step is:

$$b_C = r_{lm} = \sqrt{\frac{1 + \cos(\theta_C + \epsilon\lambda \sin(-\theta_C))}{2}} \quad (3.4)$$

Accordingly, the cost that  $C$  incurs can be written as (Eq. 2.14):

$$c = \alpha \frac{|\dot{\theta}_l(t + \epsilon) - \dot{\theta}_l(t)|}{2\pi} = \alpha \frac{|\omega_C + \epsilon\lambda \sin(\theta_C(t)) - \omega_C|}{2\pi} = \alpha \frac{|\epsilon\lambda \sin(\theta_C(t))|}{2\pi} \quad (3.5)$$

Considering a mean-field scenario, we can assume that  $\theta_C(t) = \frac{\pi}{2}$  since  $\theta_D(t) = 0$ . Hence, the benefit increase  $b$  due to cooperation and the cost  $c$  are given by:

$$b = b_C - b_D = \sqrt{\frac{1 + \cos(\frac{\pi}{2} - \epsilon\lambda \sin(\frac{\pi}{2}))}{2}} - \sqrt{\frac{1 + \cos(\frac{\pi}{2})}{2}} = \frac{\sqrt{2 + 2\sin(\epsilon\lambda)} - \sqrt{2}}{2} \quad (3.6)$$

$$c = \alpha \frac{|\epsilon\lambda \sin(\frac{\pi}{2})|}{2\pi} = \frac{\alpha\epsilon\lambda}{2\pi} \quad (3.7)$$

Applying the method of [19], the necessary condition  $b/c > \langle k \rangle$  under which cooperation can emerge translates in:

$$\frac{\sqrt{2 + 2\sin(\epsilon\lambda)} - \sqrt{2}}{\epsilon\lambda\langle k \rangle} > \alpha \quad (3.8)$$

The last inequality allows to perimeter the region of the parameter space  $(\alpha, \lambda)$  where cooperation has the possibility to thrive.

### 3.2. Static networks

We begin the computational study of the EKD model on the static topologies ER and RGG. The objective of this analysis is to reproduce the results presented by Antonioni *et al.* in [6].

We aim to evaluate the coevolution of synchronization and cooperation across various parameter configurations, each representing a different evolutionary landscape. Let us remind the reader that the parameter space encompasses two control parameters, the coupling strength  $\lambda$  and the relative cost  $\alpha$  (sec. 2.3).

To inspect whether an absorbing state is reached, we initialize the simulation as described in sec. 2.5 and we let the system evolve over time until it attains the stationary state, testing different pairs of  $\lambda$  and  $\alpha$ . We repeat this procedure several times to average out the stochasticity of the single realizations. The stationary state is examined in terms of both synchronization level, assessed globally through  $r_G$  (Eq. 2.2), and locally through  $r_L$  (Eq. 2.8), as well as cooperation level represented by  $C$ . This method allows us to construct a phase diagram for the three order parameters. Fig. 3.1 resumes the outcome of intensive numerical simulations following this approach.

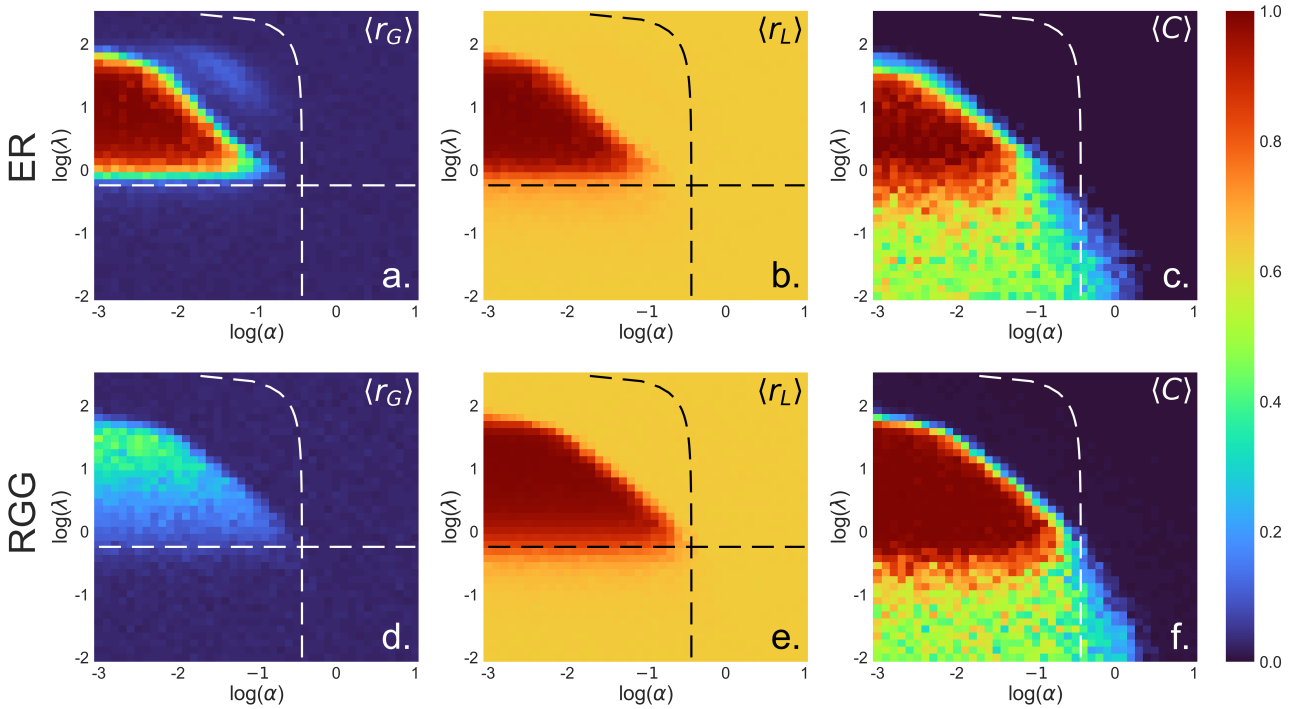


Fig. 3.1. ER and RGG phase diagram for a networked population of  $N=1000$  oscillators/agents. From left to right, each column illustrates the average level of global synchronization  $\langle r_G \rangle$ , local synchronization  $\langle r_L \rangle$  and cooperation  $\langle C \rangle$  as a function of the coupling  $\lambda$  and relative cost  $\alpha$  in logarithmic scale. The top row corresponds to ER topology, the bottom one to RGG topology. Averages are performed over 50 different realizations.

*ER analysis.* We first focus on the top row of Fig. 3.1. At first sight, it is immediately evident the strong correlation between the onset of cooperation and synchronization in ER topology.

For low and intermediate values of  $\alpha$ , the system experiences a phase transition from a completely incoherent state to a fully synchronized one, both at global and local scale (panels a. and b.). This transition occurs for values of the coupling  $\lambda$  slightly higher than the theoretical critical value  $\lambda_c^{th}$  for the "without-game" model (Eq. 2.9), displayed as a horizontal dashed line. The emergence of

coherence is complemented by the triumph of cooperation against defection (panel c.). This seems intuitive as we are examining the region of the parameter space where the analytical condition derived in sec. 3.1 holds—the area delimited by the curved dashed line—, where cooperation is theoretically fostered. However, although the cheap regime, cooperation thrives only when  $\lambda$  exceeds the critical value for the coherent state, indicating a profound intertwining of the two dynamics. This is an exemplary case of what *coevolving* truly means.

Interestingly, the system exhibits another phase transition as the coupling increases, spontaneously loosing synchronization. The reason behind this behavior lies in the excessively high variation of the angular frequency  $\dot{\theta}_i$  during the discrete dynamics, caused by the large values of  $\lambda$ . Such a variation leads to an unsustainable cost for the cooperators with respect to the benefit gained by the increased synchronization. As a result, the system collapses in a fully incoherent state of defectors.

Similarly, for high values of  $\alpha$ , the interaction costs are so high that synchronization and cooperation are never achieved, regardless of the coupling strength. The region where defection is favoured—the region delimited by the dashed curved according to the inequality 3.8— corroborates this result.

As a final remark, we note that our theoretical argument regarding the lower bound for  $r_L$  computed in Sec. 3.1 is confirmed, since the microscopic order parameter approaches  $\overline{r_{lm}}$  when incoherence dominates (panel b.).

*RGG analysis.* The population exhibits significantly different behavior on RGG topology (Fig. 3.1 - bottom row) compared to the ER case. Here, although cooperation emerges over a larger portion of the parameter space (panel f.), the system never converges towards global synchronization (panel d.). Conversely, local synchronization coevolves with cooperation (panel e.), suggesting that each oscillator is synchronized with its neighbourhood. The cause of this intriguing discrepancy lies in the structure of the RGG topology. Unlike ERs, RGGs exhibits strong spatial correlations, meaning that edges are assigned so that the population organizes in clusters. The presence of community structures implies that nodes interact mainly within their own cluster, hence global synchronization is not achieved due to the poor communication among the different communities, even when the whole population cooperates. This phenomenon highlights the significant impact of topology on the system's dynamics.

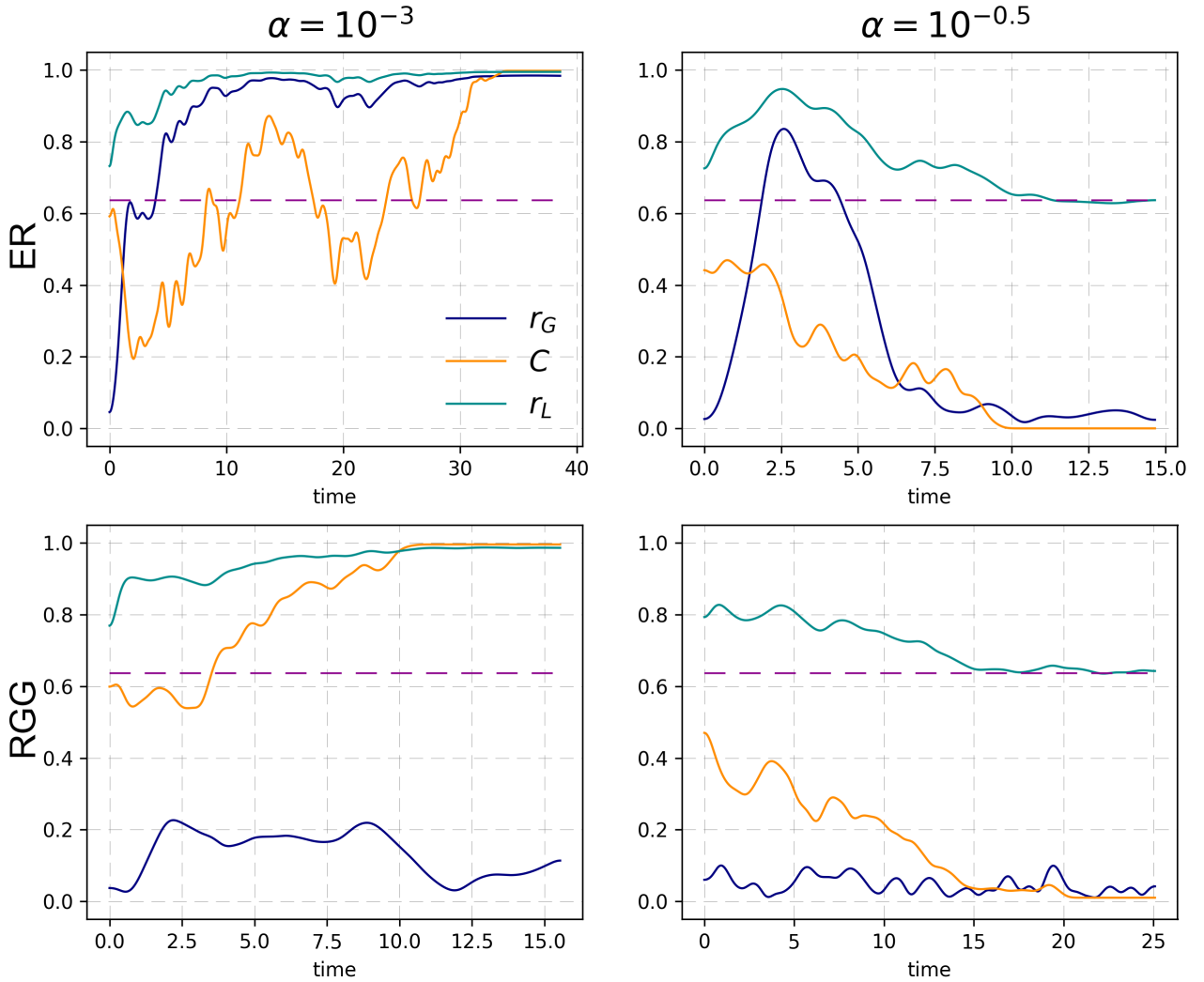
Ultimately, let us stress once more the drastic interplay between synchronization and cooperation dynamics in the EKD model by examining the single simulations over time.

On one side, it is quite straightforward to figure out why cooperating is necessary to promote synchronization: the Kuramoto dynamics comes out only if the nodes decide to collaborate ( $s_i = 1$ ), meaning that a fully cooperative state will bring the system at least to local synchronization in a suitable regime.

Conversely, it is more subtle to understand whether a fully synchronized state leads always to the onset of cooperation. This may occur because a defector surrounded by cooperators has no incentive to change its strategy. The defector receives the benefits from its cooperative neighbors without incurring any cost itself. However, if interactions are sufficiently cheap, the neighboring cooperators will incur progressively lower cost over time, leading to higher payoffs compared to the defector since more synchronized. The increasing synchrony among cooperators potentially persuades the defector to change its strategy, resulting in a cluster entirely composed of cooperators.

Actually, the transient behavior of the single dynamics is unpredictable, resulting in diverse evolutionary paths even for two realizations in the same identical scenario.

In Fig. 3.2, the single-realization time evolution of the three order parameters is depicted for both the low-cost interaction regime ( $\alpha = 10^{-3}$ ) and the high-cost interaction regime ( $\alpha = 10^{-1}$ ). The right column elucidates the previously mentioned argument: cooperation (orange line) is driven by synchronization (blue/cyan lines) when the cost of interaction is low. Notably, as discussed earlier, the macroscopic order parameter  $r_G$  never reaches high values in the bottom-left panel due to topological effects. In the left column, despite the coupling value favoring synchronization,  $\lambda = 4$ , the system collapses into an incoherent state of defectors because the cost of interaction is excessively high.



. The theoretical value  $\overline{r_{lm}}$  is displayed by the horizontal dashed line.

Fig. 3.2. Time evolution in different regimes. Each panel displays the trajectories of the three order parameters  $r_G$  (blue),  $r_L$  (cyan),  $C$  (orange) over time. The top(bottom) row corresponds to the ER(RGG) topology. The first column portrays the cheap interaction scenario  $\alpha = 10^{-3}$ , whereas the second column stands for the expensive regime  $\alpha = 10^{-0.5}$ . The coupling is commonly set to  $\lambda = 4$ .

### 3.3. Temporal proximity graphs

The absence of a global coherent state in the RGG topology raises the question of whether a fully synchronized state can be achieved despite the presence of strong spatial correlations that force the population to primarily interact within sub-communities. To address this question, it is reasonable to consider the role of time as a potential game-changer. If the members of the population can change their neighbors over time, they may be able to overcome the spatial constraint and promote a fully synchronized state. To explore this intuition, we investigate the behavior of the EKD model on TPGs. The reason behind the choice of this topology is to preserve the connectivity features of the static RGG network as much as possible in the new analysis: TPGs interaction pattern, indeed, is shaped keeping the same spatial correlations of RGGs at each time step.

Before beginning the analysis, it is important to note that for TPGs, an additional control parameter comes into play, i.e. the relative mobility  $\mu$ , which represents the ratio between the speed of the agents  $v$  and the distance threshold of interaction  $R$  (see subsec. 2.4.3). This variable allows us to tune the system across different mobility regimes: from a situation of *low-mobility*, characterized by values of  $v \ll R$  to a *high-mobility* regime where  $v \gg R$ . In a low-mobility scenario agents move very slowly away from their randomly assigned initial position, whereas in the high-mobility regime agents rapidly traverse the space from one side to another.

For the sake of simplicity, since our aim is to assess the onset of synchronization, we keep the coupling strength constant at the favorable value  $\lambda = 10$  for the rest of the analysis. As a result, it is possible to explore the behavior of the networked population across various levels of interaction cost and nodes' mobility, which is the primary interest of this investigation.

*TPG phase diagram.* Following the same approach introduced in Sec. 3.2, we construct the phase diagram of the EKD model on TPG networks varying the relative cost  $\alpha$  and the relative mobility  $\mu$ . The remarkable outcome of comprehensive numerical simulations is portrayed in Fig. 3.3.

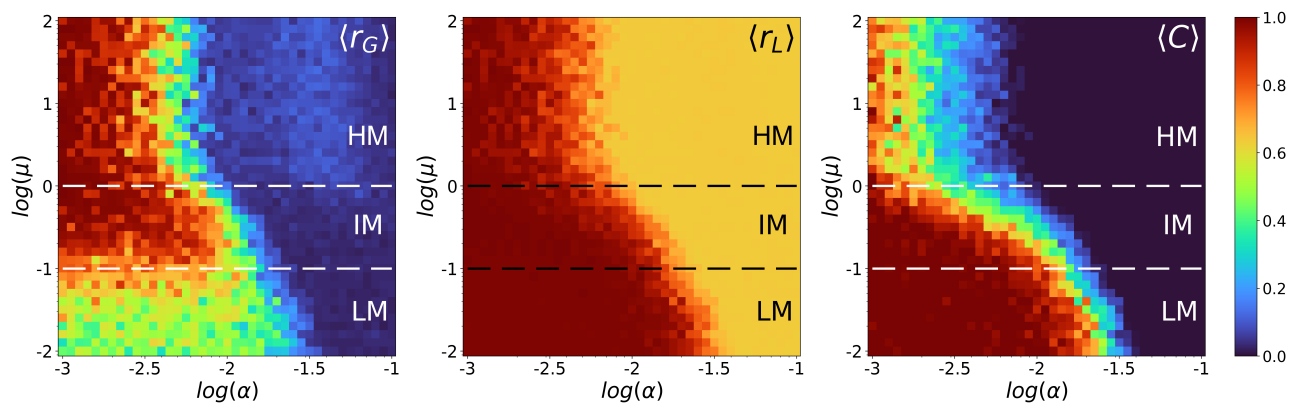


Fig. 3.3. TPG phase diagram for a networked population of  $N = 1000$  oscillators/agents. From left to right, each panel displays the behavior of the macroscopic(microscopic) order parameter  $\langle r_G \rangle(\langle r_L \rangle)$  and the cooperation  $\langle C \rangle$ , for different values of the relative cost(mobility)  $\alpha(\mu)$  in logarithmic scale. Three different regions are identified: the LM, IM and HM regimes are delimited by the horizontal dashed lines  $\mu = 0.1$  and  $\mu = 1$ . The latter corresponds to the critical value of the speed  $v = R$  (subsec. 2.4.3). Averages are performed over 10 realizations.

From the picture, we immediately recognize that, unlike the RGG case, TPG topology admits the onset of global synchronization when the relative mobility  $\mu$  exceeds a certain critical threshold (left-panel). Accordingly to the static cases, this transition is possible only for relatively low values of  $\alpha$ , as in the expensive interaction domain the system falls into an incoherent stationary state regardless the value of  $\mu$ .

Let us examine the diagram in more details. Focusing on the low cost region, the following three different regimes can be identified:

**a. Low mobility regime (LM)** For low values of  $\mu$ , the motion of the oscillators is so restricted that the system behaves similarly to the static RGG case. The initially formed clusters preserve their structure over time, with each agent interacting essentially with the same neighbors during the whole dynamics. Therefore, only local synchronization is attained despite the emergence of cooperation.

**b. Intermediate mobility regime (IM)** The interesting novel outcome occurs as the value of  $\mu$  increases (within the range  $0.1 < \mu < 1$ ). The population succeeds in achieving global synchronization. In this scenario, each oscillator can explore a large enough portion of space to interact with a significant number of different partners, collecting the phase information of the fellow passengers and adjusting its rhythm accordingly. Evidently, as in the previous cases, cooperation is essential to reach such a collective behavior, meaning that the two aspects coevolve, mutually reinforcing each other.

**c. High mobility regime (HM)** The most intriguing and enigmatic behaviour arises when the value of  $\mu$  becomes excessively high. As soon as the relative mobility approaches and surpasses the critical value of  $\mu = 1$  (dashed line in Fig.3.3), the phase diagram shows a visible *bottleneck*, i.e. a dramatic reduction of the parameter space region favoring synchronization, but particularly cooperation. Intuitively, this unprecedented phenomenology is correlated to the disproportionate capability of motion of the agents. The higher the value of  $\mu$ , i.e. the greater the speed  $v$  compared to  $R$ , the farther the agents travel beyond their own spatial range of interaction at each time step. As a result, each oscillator continuously changes all its neighbors, interactions are too brief to get synchronized, hence the accumulated benefit is too low compared to the cost it would incur.

The emergence of synchronization for a considerably large range of the relative cost, despite the substantial absence of a cooperative state, remains an open question at this stage. Subsequently, we will provide potential insights to tackle this problem.

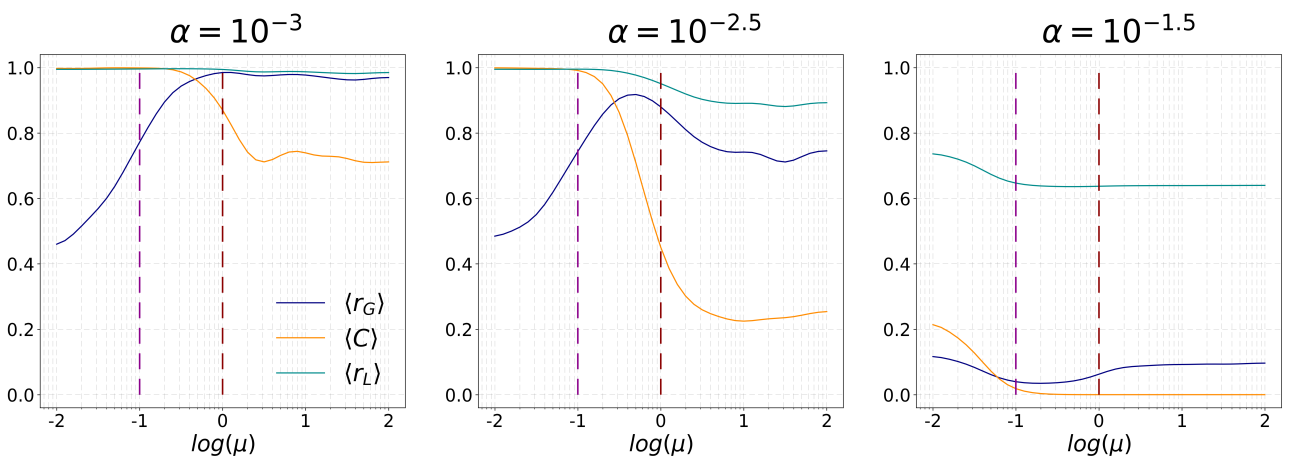


Fig. 3.4. Phase diagram sections from cheap to expensive interaction regimes. The trends of  $\langle r_G \rangle$ ,  $\langle r_L \rangle$ ,  $\langle C \rangle$  are displayed as a function of the relative mobility  $\mu$ , for  $\alpha = 10^{-3}$  (cheap),  $\alpha = 10^{-2.5}$  (intermediate),  $\alpha = 10^{-1.5}$  (expensive). The LM, IM and HM regimes are separated by the two vertical dashed lines.

To better highlight the aforementioned partition of the TPG phase diagram, we inspect the behavior of the order parameters by selecting three representative values of  $\alpha$ . The sections, shown in Fig. 3.4, elucidate the interplay of the cost and the mobility.

For very low values of  $\alpha$  (left panel), the system exhibits only one phase transition from incoherence to synchronization, which occurs close to the critical mobility  $\mu = 1$  (dashed line), maintaining it regardless the increasing  $\mu$ . Even cooperation remains sufficiently high as the costs are very low.

The middle panel, conversely, points out that even a relatively small increase of the interaction cost leads to a totally different outcome. Here, we can distinguish the IM domain, being the only one where  $\langle r_G \rangle$  and  $\langle C \rangle$  both spontaneously emerge. This section considers a region outside the previously mentioned "bottleneck". Consequently cooperation drops drastically while approaching the HM domain, eventually reaching levels indicative of near-total defection.

For the sake of completeness, the right panel underlines once more the utter absence of collective behaviors when the cost increases excessively.

*Temporal dynamics.* The conclusion of our analysis aims to offer promising intuitions to shed light on the mechanisms governing the EKD dynamics in the HM regime. In this perspective, the sole inspection of the stationary state is hardly exhaustive.

Therefore, we conducted several different simulations of the entire dynamics over time and compared the findings on the HM scenario with those of the other domains in the same interaction cost landscape. Fig. 3.5 illustrates a typical realization for each regime.

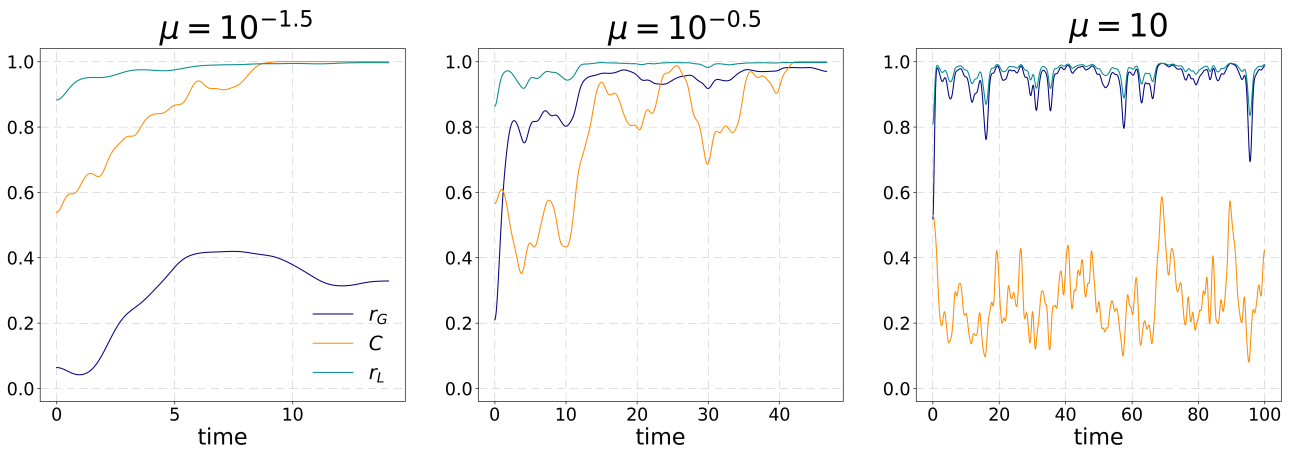


Fig. 3.5. Time evolution in the various regimes. From the left, typical temporal dynamics of the three order parameters  $\langle r_G \rangle$ ,  $\langle r_L \rangle$ ,  $\langle C \rangle$  for  $\mu = 10^{-1.5}$  (LM),  $\mu = 10^{-0.5}$  (IM),  $\mu = 10$  (HM). The relative cost is fixed to the interesting value of  $\alpha = 10^{-2.5}$ .

Referring to the displayed simulations as exemplary cases, it is evident that they exhibit significant diversity. The dynamics in LM and IM regimes (left and middle panels) differ, as the full synchronization is attained only for intermediate values of  $\mu$ . Nevertheless, they share a fundamental characteristic: in both cases cooperation is an absorbing state.

On the contrary, the time evolution in the HM regime shows that the fraction of cooperators fluctuates depending on the single realization, often falling below half of the population. This enigmatic collective behavior translates in the possibility for the few cooperators of the population to meet the majority of the defectors along their path and bear the cost that, in the other scenarios, the majority of

the population would share. This novel evidence may suggest that such a scenario allows the population to achieve full synchronization while incurring a much lower overall cost.

However, the noisy trajectory of  $C$  also reveals the unstable nature of the system in the HM regime, being extremely sensitive to little perturbations due to stochastic unexpected events or to initial conditions. Hence, by letting the system evolve for a longer time, we expect it will eventually reach a stationary state, but the outcome of the temporal evolution, whether cooperation/coherence or defection/incoherence, is unpredictable. As a matter of fact, the phenomenology of the HM regime reminds to the one of a chaotic system.

## 4. CONCLUSION

Synchronization —the most exemplary manifestation of nature’s order— and cooperation —the indispensable behavioral mechanism to guarantee the welfare of a community— appear to be two sides of the same coin. The Evolutionary Kuramoto Dilemma aims to capture this profound interplay and provides a methodology to study the coevolution of the two phenomena on networked population.

To summarize, we primarily investigated the EKD behavior on static networks (ERs and RGGs), enlightening how the choice of the topology drastically affects the eventual outcome of the dynamics. Strong spatial correlations prevent the onset of a global coherent state, despite they favour the emergence of cooperation.

The main purpose of our work was to overcome the lack of global synchronization in spatial networks, by identifying time as the potential missing link. Therefore, we conducted the novel exploration on spatio-temporal networks, particularly on TPGs, in search of the onset of a coherent state.

The results of intensive numerical simulations were even more surprising than the expectations, opening a wide range of questions and avenues for further research. TPG phase diagram not only displays a phase transition towards full synchronization, but it also demonstrates a variegated phenomenology depending on the level of mobility each agent incurs. At first glance, the IM regime fully meets our initial requirement to obtain the spontaneous emergence of both synchronization and cooperation.

HM one is certainly the most intriguing mobility regime. On one side, the loss of cooperation suggests that synchronization can be reached by incurring in a much smaller amount of cost. On the other hand, the temporal dynamics in this regime indicates that, de facto, the system becomes chaotic.

Although various variants and applications of EKD model have been proposed since 2017, this work is, to our knowledge, the first extension of the model on spatio-temporal networks.

Various future improvements could be conducted along this direction. In the first place, a better characterization of the HM regime looks to be required. Longer-time simulations could lead to valuable understandings of the instability of the system. Ideally, a rigorous stability analysis would be asked for a complete comprehension of EKD behavior in this domain.

An evident potential advancement is the analysis of EKD on different spatio-temporal networks rather than TPGs. Taking inspiration from the "without-game" case, ad-hoc spatio-temporal networks yield to the emergence of surprising phenomena such as *explosive synchronization* [20] [21]. Exploring diverse nodes’ motion rules, employing different timescales between dynamics and mobility, or considering adaptive couplings are all promising candidates to find out even a richer phenomenology. Ultimately, looking further ahead, the end goal of EKD is certainly to describe real-world scenarios where the interplay of synchronization and cooperation is particularly relevant. In this perspective, EKD on spatio-temporal network can be seen as a potential variant to describe biological, social, robotic *oscillators that swarm and sync* [22].

## BIBLIOGRAPHY

- [1] A. Pikovsky, M. Rosenblum, and J. Kurths, *Synchronization: A Universal Concept in Nonlinear Sciences* (Cambridge Nonlinear Science Series). Cambridge University Press, 2001.
- [2] J. A. Acebrón, L. L. Bonilla, C. J. Pérez Vicente, F. Ritort, and R. Spigler, “The kuramoto model: A simple paradigm for synchronization phenomena,” *Rev. Mod. Phys.*, vol. 77, pp. 137–185, 1 Apr. 2005. doi: [10.1103/RevModPhys.77.137](https://doi.org/10.1103/RevModPhys.77.137). [Online]. Available: <https://link.aps.org/doi/10.1103/RevModPhys.77.137>.
- [3] M. Nowak, *Evolutionary Dynamics: Exploring the Equations of Life*. Harvard University Press, 2006. [Online]. Available: <https://books.google.es/books?id=YXrIRDuAbE0C>.
- [4] G. Szabó and G. Fáth, “Evolutionary games on graphs,” *Physics Reports*, vol. 446, no. 4, pp. 97–216, 2007. doi: <https://doi.org/10.1016/j.physrep.2007.04.004>. [Online]. Available: <https://www.sciencedirect.com/science/article/pii/S0370157307001810>.
- [5] S. Boccaletti, V. Latora, Y. Moreno, M. Chavez, and D.-U. Hwang, “Complex networks: Structure and dynamics,” *Physics Reports*, vol. 424, no. 4, pp. 175–308, 2006. doi: <https://doi.org/10.1016/j.physrep.2005.10.009>. [Online]. Available: <https://www.sciencedirect.com/science/article/pii/S037015730500462X>.
- [6] A. Antonioni and A. Cardillo, “Coevolution of synchronization and cooperation in costly networked interactions,” *Physical Review Letters*, vol. 118, p. 238 301, Jun. 2017. doi: [10.1103/PhysRevLett.118.238301](https://doi.org/10.1103/PhysRevLett.118.238301).
- [7] S. H. Strogatz, “From kuramoto to crawford: Exploring the onset of synchronization in populations of coupled oscillators,” *Physica D: Nonlinear Phenomena*, vol. 143, no. 1, 2000. doi: [https://doi.org/10.1016/S0167-2789\(00\)00094-4](https://doi.org/10.1016/S0167-2789(00)00094-4). [Online]. Available: <https://www.sciencedirect.com/science/article/pii/S0167278900000944>.
- [8] A. Arenas, A. Díaz-Guilera, J. Kurths, Y. Moreno, and C. Zhou, “Synchronization in complex networks,” *Physics Reports*, vol. 469, no. 3, 2008. doi: <https://doi.org/10.1016/j.physrep.2008.09.002>. [Online]. Available: <https://www.sciencedirect.com/science/article/pii/S0370157308003384>.
- [9] D. M. Abrams and S. H. Strogatz, “Chimera states for coupled oscillators,” *Phys. Rev. Lett.*, vol. 93, p. 174 102, 17 Oct. 2004. doi: [10.1103/PhysRevLett.93.174102](https://doi.org/10.1103/PhysRevLett.93.174102). [Online]. Available: <https://link.aps.org/doi/10.1103/PhysRevLett.93.174102>.
- [10] J. G. Restrepo, E. Ott, and B. R. Hunt, “Onset of synchronization in large networks of coupled oscillators,” *Phys. Rev. E*, vol. 71, p. 036 151, 3 Mar. 2005. doi: [10.1103/PhysRevE.71.036151](https://doi.org/10.1103/PhysRevE.71.036151). [Online]. Available: <https://link.aps.org/doi/10.1103/PhysRevE.71.036151>.
- [11] P. Erdős and A. Rényi, “On random graphs i,” *Publicationes Mathematicae Debrecen*, vol. 6, p. 290, 1959.

- [12] M. Barthélemy, “Spatial networks,” *Physics Reports*, vol. 499, no. 1–3, pp. 1–101, Feb. 2011. doi: [10.1016/j.physrep.2010.11.002](https://doi.org/10.1016/j.physrep.2010.11.002). [Online]. Available: <http://dx.doi.org/10.1016/j.physrep.2010.11.002>.
- [13] J. Dall and M. Christensen, “Random geometric graphs,” *Phys. Rev. E*, vol. 66, p. 016 121, 1 Jul. 2002. doi: [10.1103/PhysRevE.66.016121](https://doi.org/10.1103/PhysRevE.66.016121). [Online]. Available: <https://link.aps.org/doi/10.1103/PhysRevE.66.016121>.
- [14] A. Antonioni and M. Tomassini, “Degree correlations in random geometric graphs,” *Phys. Rev. E*, vol. 86, p. 037 101, 3 Sep. 2012. doi: [10.1103/PhysRevE.86.037101](https://doi.org/10.1103/PhysRevE.86.037101). [Online]. Available: <https://link.aps.org/doi/10.1103/PhysRevE.86.037101>.
- [15] P. Holme and J. Saramäki, “Temporal networks,” *Physics Reports*, vol. 519, no. 3, pp. 97–125, 2012, Temporal Networks. doi: <https://doi.org/10.1016/j.physrep.2012.03.001>. [Online]. Available: <https://www.sciencedirect.com/science/article/pii/S0370157312000841>.
- [16] D. Ghosh *et al.*, “The synchronized dynamics of time-varying networks,” *Physics Reports*, vol. 949, pp. 1–63, 2022, The synchronized dynamics of time-varying networks. doi: <https://doi.org/10.1016/j.physrep.2021.10.006>. [Online]. Available: <https://www.sciencedirect.com/science/article/pii/S0370157321004166>.
- [17] S. Meloni *et al.*, “Effects of mobility in a population of prisoner’s dilemma players,” *Phys. Rev. E*, vol. 79, p. 067 101, 6 Jun. 2009. doi: [10.1103/PhysRevE.79.067101](https://doi.org/10.1103/PhysRevE.79.067101). [Online]. Available: <https://link.aps.org/doi/10.1103/PhysRevE.79.067101>.
- [18] A. Antonioni and A. Cardillo, Supplementary material for the manuscript: “Coevolution of Synchronization and Cooperation in Costly Networked Interactions”, 2017. [Online]. Available: <http://link.aps.org/supplemental/10.1103/PhysRevLett.118.238301>.
- [19] H. Ohtsuki, C. Hauert, E. Lieberman, and M. Nowak, “A simple rule for the evolution of cooperation on graphs and social networks,” *Nature*, vol. 441, pp. 502–5, May 2006. doi: [10.1038/nature04605](https://doi.org/10.1038/nature04605).
- [20] X. Ling, W.-B. Ju, N. Guo, C.-Y. Wu, and X.-M. Xu, “Explosive synchronization in network of mobile oscillators,” *Physics Letters A*, vol. 384, no. 35, p. 126 881, 2020. doi: <https://doi.org/10.1016/j.physleta.2020.126881>. [Online]. Available: <https://www.sciencedirect.com/science/article/pii/S0375960120307489>.
- [21] S.-F. Ma, H. Bi, Y. Zou, Z.-H. Liu, and S.-G. Guan, “Shuttle-run synchronization in mobile ad hoc networks,” *Frontiers of Physics*, vol. 10, May 2015. doi: [10.1007/s11467-015-0475-z](https://doi.org/10.1007/s11467-015-0475-z).
- [22] K. O’Keeffe, H. Hong, and S. Strogatz, “Oscillators that sync and swarm,” *Nature Communications*, vol. 8, Nov. 2017. doi: [10.1038/s41467-017-01190-3](https://doi.org/10.1038/s41467-017-01190-3).